JOURNAL OF MATERIALS SCIENCE 26 (1991) 559–568

Ageing characteristics of dendritic and non-dendritic (stir-cast) Zn–Al alloy (ZA-27)

H. LeHUY
Industrial Materials Research Institute, National Research Council Canada, 75 De Mortagne Blvd, Boucherville, Quebec J4B 6Y4, Canada

G. L'ESPÉRANCE
Department of Metallurgical Engineering, Ecole Polytechnique de Montréal, PO Box 6079, Succ. "A" Montreal, Quebec H3C 3A7, Canada

The dimensional changes of dendritic and non-dendritic (stir-cast) Zn–Al alloy (ZA-27) were investigated during ageing at temperatures in the range 20–245 °C. The linear expansion of both dendritic and non-dendritic samples increased rapidly with ageing time after about 24 h at 95 °C. An initial normalization treatment led to a large initial growth of the alloy which increased further after prolonged ageing times ($\geq 10^4$ h). Accelerated ageing tests in the range 75–250 °C showed that increasing the ageing temperature decreased the long term linear expansion of the alloy. In comparing the behaviour of the two materials, the stir-cast material grew less than the dendritic alloy. Extensive SEM and TEM done on as-stir-cast and aged samples showed that the main changes during ageing occurred in the α (FCC) lamellae of the $\beta \rightarrow \alpha +$ (Zn) eutectoid, the α phase at the primary $\alpha_{particles}/\beta_{eutectoid}$ interface and in the interparticle areas. In the α lamellae and at the interface, zinc precipitated whilst the τ′ phase precipitated in the interparticle areas. It is considered that the occurrence of this latter phase, rich in copper, is responsible for the growth of stir-cast material during ageing.

1. Introduction

Among the zinc–aluminium foundry alloys, ZA-27 exhibits attractive physical and mechanical properties combined with good friction and wear resistance properties making it a choice alloy for a multitude of end-use applications. As some of these applications require increased performance of the alloy at high temperature, in particular its dimensional stability, intensive investigations [1] have been done to develop high quality products. Recently, non-conventional casting processes, such as stir-casting (or rheo-casting) [2–5] and compo-casting [6, 7] were investigated for ZA-27 taking advantage of this alloy's wide freezing range. As the solidification conditions of these techniques are not standard, a different behaviour of the microstructure of the alloy was reported.

The microstructural changes of the binary Zn–Al alloy during ageing already have been followed by Lecomte-Beckers *et al.* [8]. Their work pointed out a multi-stage decomposition of supersaturated solid solutions. The presence of about 2 wt % copper in ZA-27 induces a complex microstructure with several metastable phases which are strongly related to the solidification conditions. X-ray analysis [9] on aged as-cast alloy revealed a multiphase decomposition with the precipitation of τ′ phase rich in copper and aluminium.

The complexity of the microstructure of stir-cast alloy, composed of degenerated dendrites embedded in a residual liquid, leads us to search further for a better understanding. Dimensional changes of both dendritic and non-dendritic (spheroidized) alloys were followed at different holding temperatures varying from room temperature to 245 °C. Their microstructural changes were studied by scanning and transmission electron microscopy. Results showed that the linear expansion of ZA-27 on ageing could be minimized in stir casting by promoting the formation of stable α phase. This paper describes the ageing behaviour of this material.

2. Experimental procedures

2.1. Material preparation

The starting material for this study was a commercial ZA-27 alloy used for casting application. Its nominal composition, solidification characteristics and phases are given in Table I. Two types of structure were selected for this investigation: a material conventionally cast in a graphite mould and a material stir cast at 470 °C. Conventional casting was carried out by melting 10-kg batches of the alloy in an electric furnace. The melt was then cast in a graphite mould with 50 ° of superheat. The castings were well insulated in order to produce an equiaxed dendritic structure as shown in Fig. 1a. On the other hand, stir casting was effected in an inert-gas-protected rheocaster with casting also

0022–2461/91 $03.00 + .12

TABLE I Characteristics of the Zn–Al alloy studied.

Base alloy	Composition of ZA-27: (in wt %) 25–28 Al; 2–2.5 Cu; 0.15 Mg; bal. zinc Temperatures: liquidus: 492 °C eutectic: 382 °C eutectoid: 275 °C		
Casting conditions	conventional	100% coarse dendrites	100–200 μm
	stir-cast 475 °C	70% fine dendrites	≤ 25
		30% primaries	100–500

in a graphite mould. Details of the stir casting technique have already been published [4]. At 470 °C, stir-cast material exhibits 30% volume primary particles as shown in Fig. 1b.

Immediately after casting, some ingots were stabilized by a normalization heat treatment of 12 h at 250 °C.

2.2. Measurements of dimensional changes

The dimensional variation of aged alloys was determined by measuring the change in length of cylindrical specimens. Accelerated ageing from 175 to 245 °C was carried out with a computerized Theta Dilatronic dilatomer on specimens 0.3 cm in diameter and 5.0 cm in length. The dimensional change was measured by an LVDT with 1% accuracy and the temperature of the holding furnace was monitored within ± 1 °C.

Ageing tests at 95 °C were conducted by placing specimens 3.8 cm in diameter and 10 cm in length in a muffle furnace. In this case, the linear expansion was measured at room temperature using a micrometer after specimens had been cooled in air. They were then replaced in the furnace for a further period of ageing. Finally, the test results were compared to reference measurements of material held at room temperature.

2.3. Scanning and transmission electron microscopy

Scanning and transmission electron microscopy (SEM and TEM) were used to characterize the phases present in each of the samples and to follow the microstructure changes which occurred during ageing. Samples for the SEM were prepared by conventional mechanical polishing techniques and observed in the unetched condition. Samples for TEM were prepared by ion beam thinning. Initially, 0.3 cm discs were ground flat on SiC paper down to a thickness of 150 μm. Micro profiles were then obtained for both faces using a micro dimpler so that the remaining thickness in the centre of the disc was considerably reduced. Final polishing in the ion beam thinner was done with a specimen holder cooled with liquid nitrogen and using both ion guns at 50° operated at 6 kV and a current of 0.2 μA. When perforation of the discs occurred, the angle was reduced to 10° so as to increase the area transparent to electrons. The overall final polishing in the ion thinner required approximately 15 h.

Backscattered electron images (BEI) in the SEM were particularly useful for identifying and rapidly locating the different phases present in the structure of the samples in view of the considerable chemical contrast difference between the various phases. Electron diffraction and X-ray microanalysis were the main methods used to identify the phases in TEM.

X-ray microanalysis in the TEM was carried out at 200 kV with a probe of similar (or smaller) size than that of the phase analysed. The net intensity was obtained using the spectrum itself to fit the background and the concentration in each element calculated using a standardless quantification program written in our laboratory based on a widely accepted procedure [10, 11]. The errors associated with such quantification procedure are in the range 5–10% [12]. Errors below 5% may have been achieved by the use of single phase standards of known composition. Such standards were not readily available for this study.

3. Results

3.1. Dimensional changes

3.1.1. Dimensional changes against ageing temperature

Fig. 2 shows the dimensional changes of dendritic and non-dendritic specimens aged at room temperature and 95 °C. Four experimental curves are presented in each graph, corresponding to different test conditions: respectively the room temperature tests on as-cast (curve A) and normalized (curve NA) materials and the 95 °C ageing tests on as-cast (curve F) and normalized (curve NF) materials. For these tests, the linear expansion was followed during 10^4 h (≈1.5 years). Data show that, for both dendritic and non-dendritic as-cast alloys, ageing at room temperature causes a slight shrinkage of 0.02% after 10^4 h (curves A); at this temperature, the stir-cast material seems more stable than the conventional ones. This feature will be discussed in detail in the next section. With regard to the tests performed at 95 °C, the curves show a similar shrinkage after 24 ageing hours followed by a pronounced expansion (curves F). On the other hand, the normalization treatment of 12 h at 250 °C, applied to both materials, induced an initial growth of about 0.09%. However, the transformation was not complete, as shown by the NF curves in which it is seen that the linear dilatation continued to increase slightly.

Accelerated ageing tests were performed at several temperatures ranging from 175 to 245 °C for times up to 100 h. The results, shown in Fig. 3 for both structures, indicate that increasing the ageing temperature decreases the long-term linear expansion of the alloy. However, above 228 °C, the linear expansion passes through a maximum, then decreases slightly. No satisfactory explanation has been given yet, but probably at high temperature two phenomena occur in opposition: the phase transformation causes the metal to expand, whereas the structural defects formed during solidification are eliminated by sintering effects, producing shrinkage. Unfortunately, during testing at

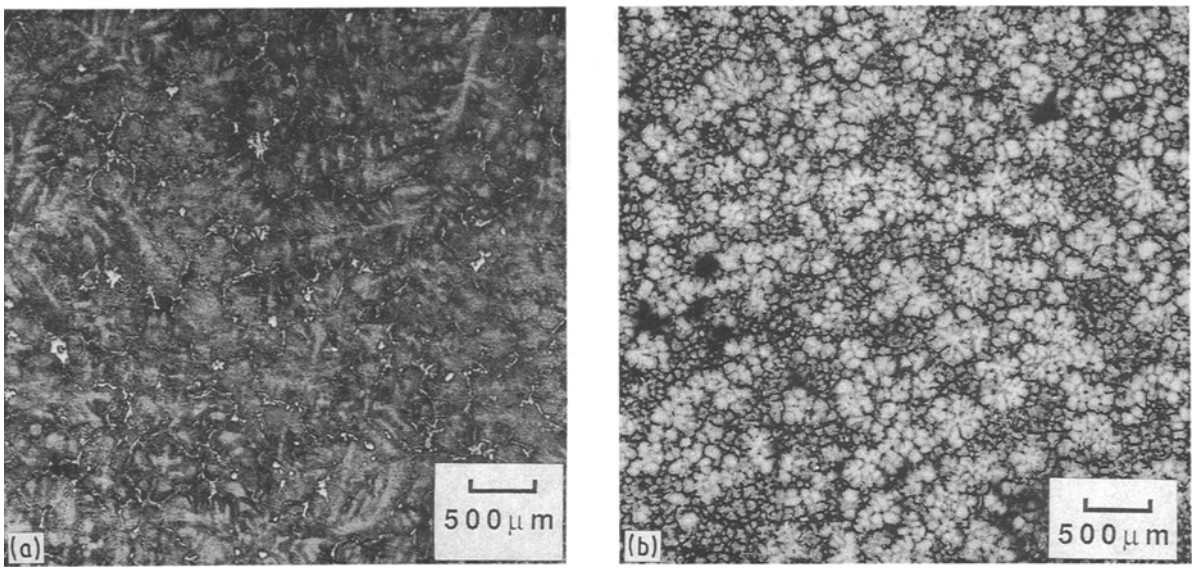

Figure 1 Microstructure of as-cast materials: (a) dendritic and (b) stir-cast.

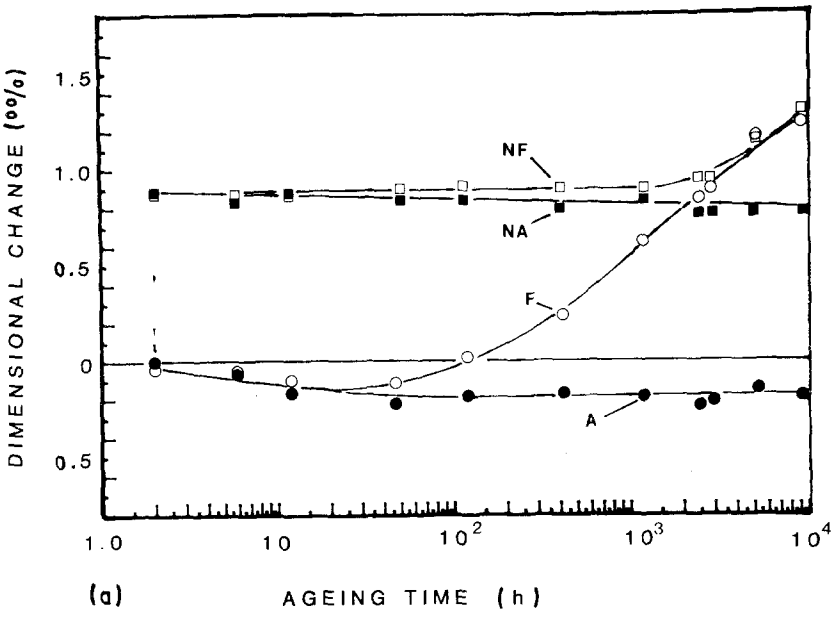

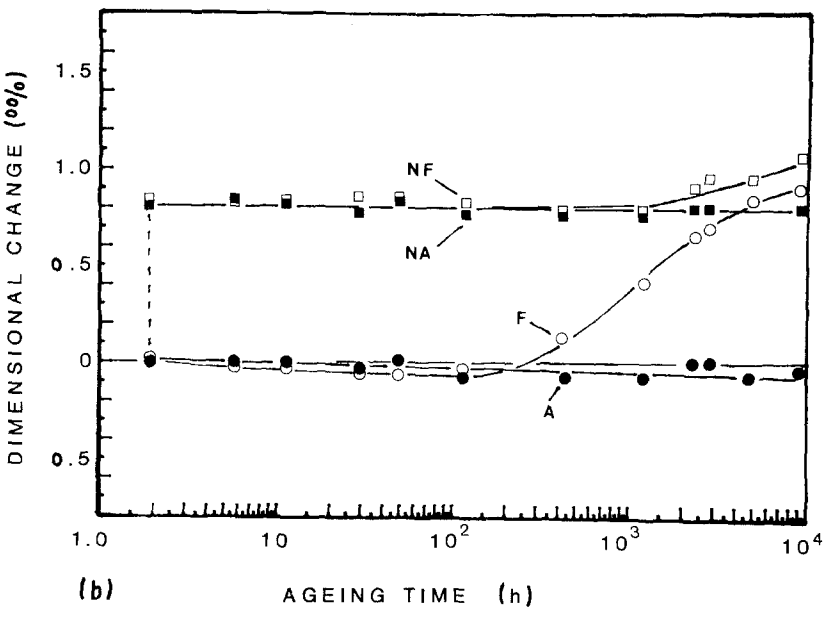

Figure 2 Dimensional changes of ZA-27 with ageing time under various test conditions: (°% means per thousand) (a) dendritic and (b) stir-cast (A) as-cast specimen, at room temperature. (F) as-cast specimen, at 95 °C. (NA): normalized specimen, at room temperature. (NF) normalized specimen, at 95 °C.

high temperature, the dimensional changes indicate the resultant of these two phenomena.

3.1.2. Dendritic against non-dendritic structure transformations

The experimental data show a slight difference between the dendritic and non-dendritic structures. Linear expansion of the dendritic specimen aged at 95 °C was about 0.14% after 10^4 h ageing while the stir-cast material expanded by 0.10% under the same conditions, as shown by the curves F in Fig. 2a and b. The same difference can be seen for the accelerated ageing tests (Fig. 3) described in the previous section. Examining the behaviour of the two types of structure, Mykura *et al.* [13] have pointed out an opposite feature, whereby it was reported that the stir-cast material grew slightly more than the dendritic one. The reasons for the distinctive contrary results are not clear, but it is possible that the different techniques of slurry production could explain this disagreement. Effectively, the two techniques adopted by Mykura and in the present work to stir the solid–liquid alloy were not the same. Moreover the important casting stage after stirring used in both cases also differed. In Mykura's work, the slurry was cast in a hot steel mould, while our material was poured in a graphite one. The cooling rate in the two cases was different. In order to clarify the process of phase transformation which induced the linear expansion, comparative microstructural studies were carried out.

3.2. Microstructural studies

3.2.1. Structure of as-cast materials

Fig. 4 shows backscattered electron images (BEI) of as-cast dendritic and non-dendritic materials, revealing the multiphase character of ZA-27. In both micrographs, the dark zone (marker G) is the α phase formed in the centre of the dendrite or the core of the primary particles. The grey zone (markers D and F) in the pictures, corresponding to the β constituent, reveals a fine lamellar structure of a eutectoid decomposition. The interdendritic or interparticle areas

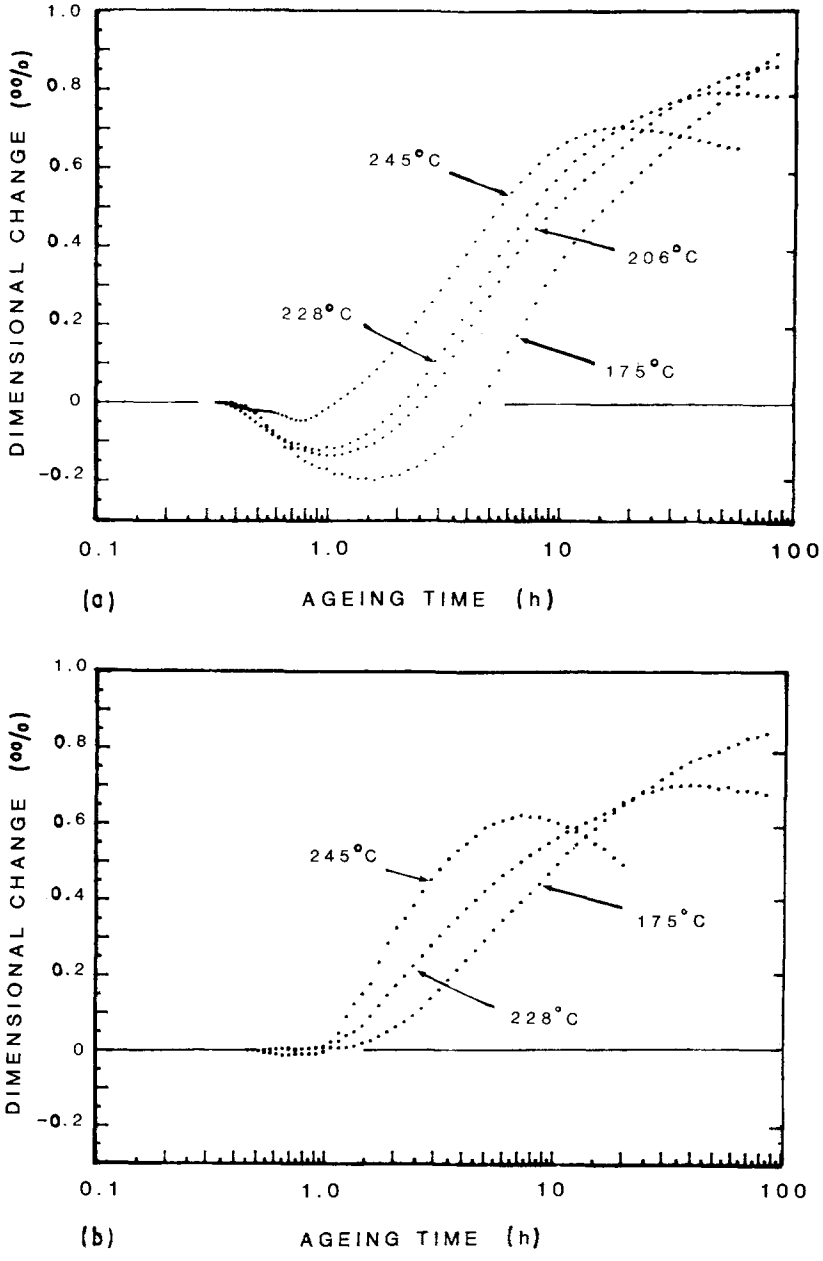

Figure 3 Dimensional changes of ZA-27 during ageing tests, respectively at 175, 206, 228 and 245 °C during 100 h: (a) dendritic and (b) stir-cast.

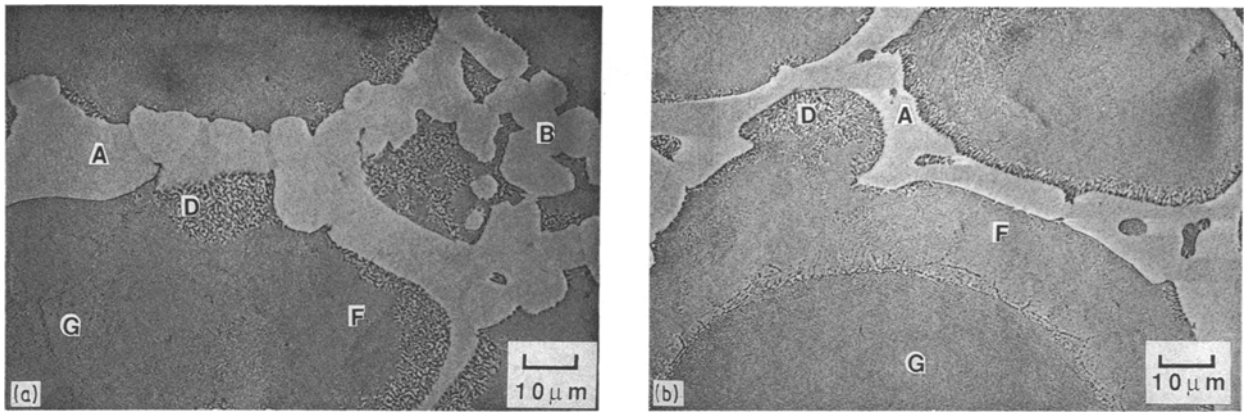

Figure 4 Backscattered electron images of as-cast materials showing the different phases present: (a) dendritic and (b) stir-cast.

(markers A and B) appearing bright in the BEI micrographs must contain large amounts of the relatively heavy elements in the alloy (Cu and Zn). The phases expected from the ternary Zn–Cu–Al phase diagram [14] are mainly the Zn rich ε ($CuZn_4$) and η (Zn) phases.

3.2.2. Normalizing effects on microstructural changes

Microstructures of normalized materials after a heat treatment at 250 °C for 12 h are shown in Fig. 5. This condition corresponds to NA treatment in Fig. 2 and is thus for samples which underwent ≈ 0.09% dilatation. The initial phases of as-cast alloys α, β, η and ε, which are formed as supersaturated phases, tended to transform into more stable phases during ageing. These transformations changed the microstructural aspect of the alloy. Coarse precipitates were observed at the interface of α/β phases (marker H), while the eutectoid structure of former β phase tended to spheroidize (markers D and F) and fine particles precipitated in the interparticle area (markers A and B). All these transformations were found to be the same to a varying degree in aged specimens. In order to describe thoroughly these phase transformations, fine microstructural and diffraction pattern analysis were undertaken with transmission electron microscopy.

3.3. Fine microstructural and diffraction pattern analysis

A TEM micrograph of a sample as stir cast is shown in Fig. 6a. The α phase (marker A) as well as the β phase (marker B) and the interface α/β can be clearly identified in the figure. Although there were some areas of the α phase for which no precipitation was observed, very extensive precipitation was generally observed in the α phase. As seen clearly at a higher magnification (Fig. 6b), most of the precipitates are thin (≈0.02 μm) and elongated (≈1.5–2.0 μm) while others are small and spherical (≈0.35 μm in diameter). The difference between the long thin images and the small spherical images can not entirely be attributed to orientation effects in the thin foil because the two morphologies were frequently observed within a single grain and that the morphology varied considerably from area to area within that grain, i.e. in certain areas most precipitates appeared elongated while in the other areas they appeared spherical.

Fig. 6c shows a composite diffraction pattern from the primary α phase and the precipitates. In this pattern, spots 1 to 6 can be indexed as the {220}

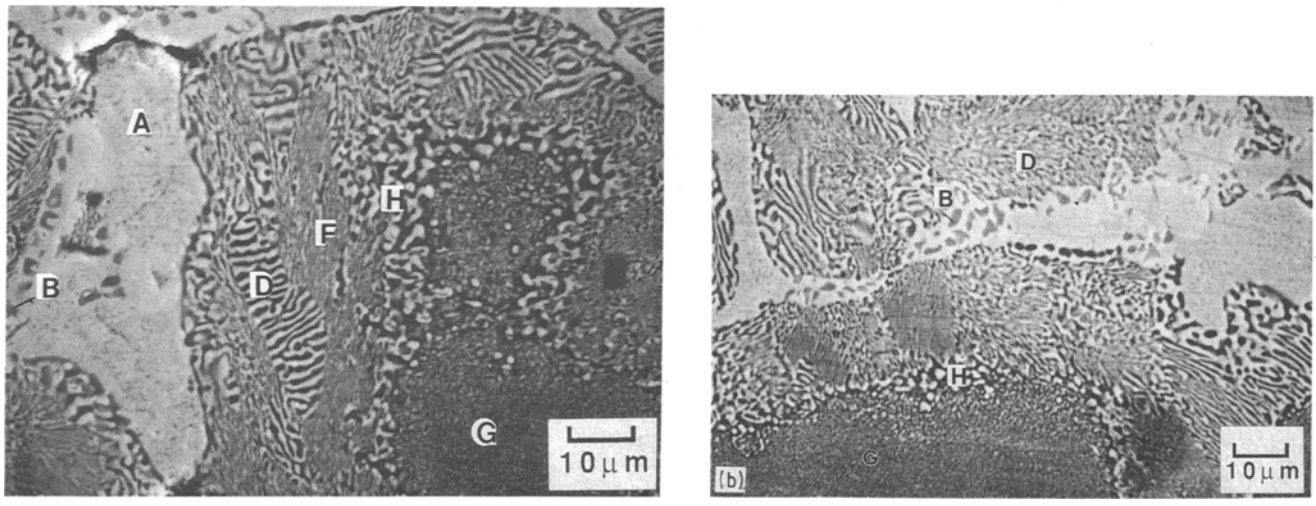

Figure 5 Backscattered electron images of normalized (250 °C for 12 h) specimens showing the transformation products: (a) dendritic and (b) stir-cast.

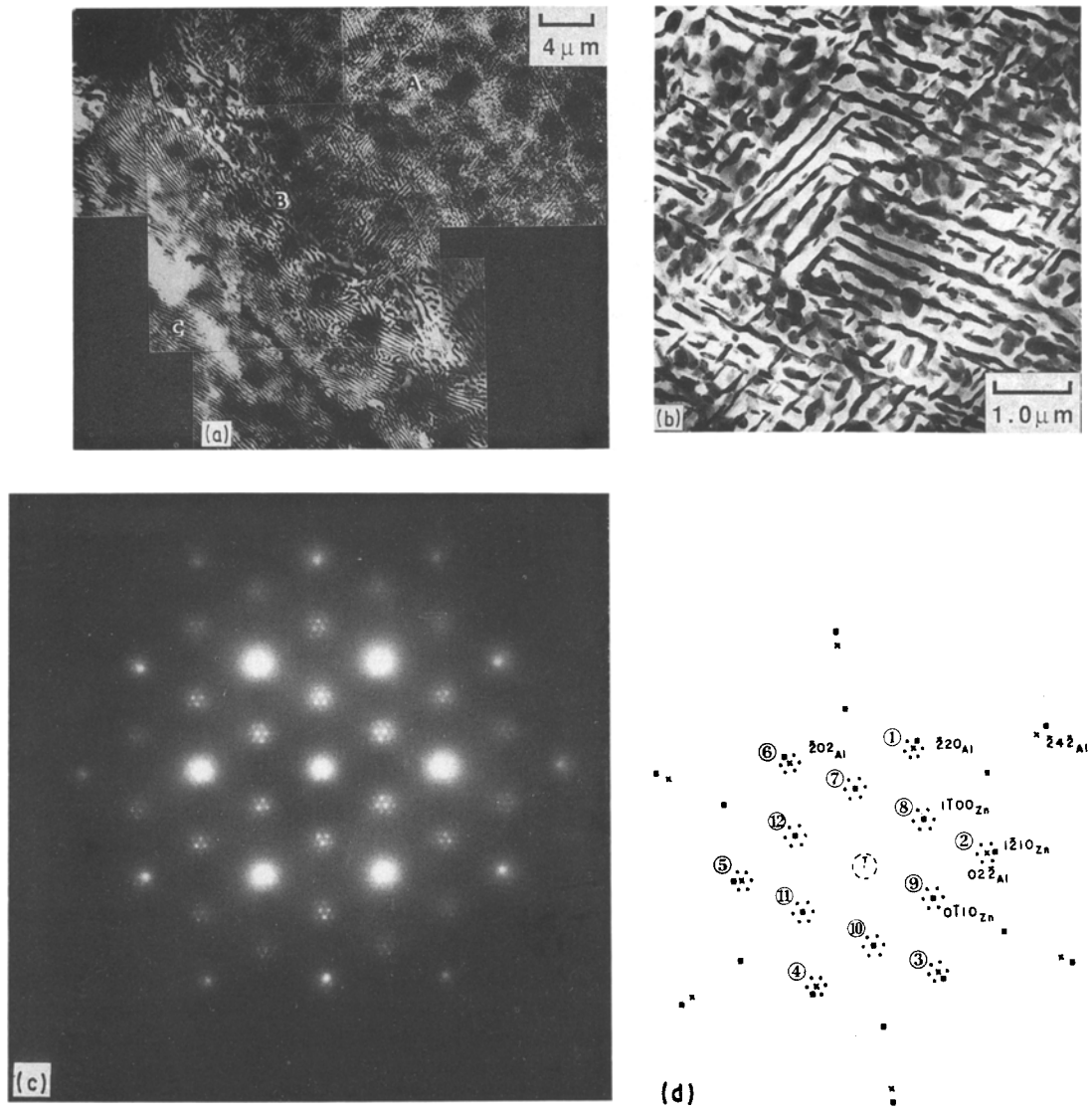

Figure 6 (a) TEM micrograph showing a general view of the structure of primary α particle (marker A), the β eutectoid (marker B) and the α/β interface (marker C) of an as-stir-cast sample. (b) Higher magnification micrograph to show the morphology of the precipitates ($g = (3\bar{3}\bar{3})$ near [1 0 1]). (c) Composite electron diffraction pattern from the α particle and the precipitates. (d) Indexation of the diffraction pattern shown in (c) (×) Al (■) Zn.

reflections of the [1 1 1] pattern of the primary aluminium-rich α phase. In addition, spots 7 to 12 can all be indexed as reflections from pure zinc constituting the [0 0 0 1] pattern of that phase. All the other satellite spots arise from double diffraction effects as shown by the fact that they disappear when tilting the specimen about an axis joining these spots to the central transmitted beam.

The coarser precipitates (≈1.5 μm and 0.02 μm wide) seen at the $\alpha_{primary}/\beta$ interface are also zinc with some copper in solution; X-ray microanalysis showed them to be 2Al–2Cu–96Zn. In assessing these compositions, account should be taken of the fact that the analyses were performed with the precipitates embedded in the aluminium matrix which will affect the results because of beam overlap onto the matrix. Nevertheless, copper was consistently detected in the precipitates while analyses of the matrix showed that it contained very little copper.

On the other hand, the lamellar structure of the β constituent is shown in Fig. 7. The crystal structure of the lamellae determined by parallel illumination electron diffraction was found to be f c c for the lamellae marked F and h c p for lamellae marked H in the micrograph. X-ray microanalysis with the results given in Table II showed that the β phase is in fact constituted of lamellae of the α (FCC, Al-rich) and η (HCP, Zn-rich) phases as expected from the binary Zn–Al phase diagram. No precipitation was observed in these lamellae contrary to the extensive precipitation seen in the primary α particles. Some α lamellae, however, had begun to transform as shown by the presence of small grains in some of the lamellae.

Finally, the interparticle area is shown to be constituted of a large number of small equiaxed grains (≈0.1 μm, Fig. 8). Microanalysis of individual grains with a small probe showed that most of the grains contained a very small amount of aluminium (≈2.0 at %) and that the Cu/Zn ratio varied from 0.13 to 0.24. The latter value corresponds to that of the $CuZn_4$ phase and it was also obtained in the case of an analysis carried out with a 0.5 μm probe

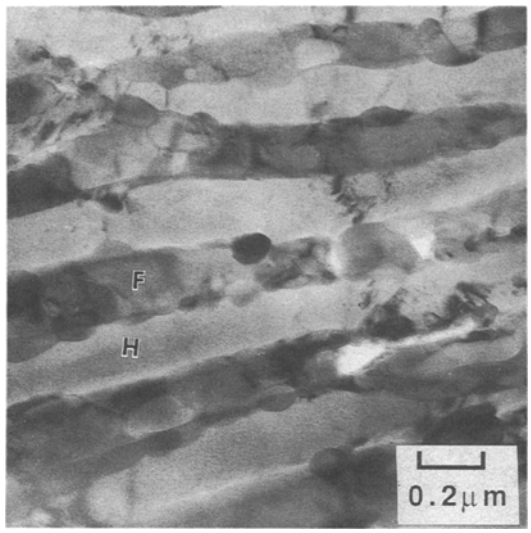

Figure 7 TEM micrograph of lamellar structure of the β eutectoid of an as-stir-cast sample.

TABLE II Results of the X-ray microanalyses.

	Phase	Al	Zn (at. %)	Cu
Lamellae of the β eutectoid before ageing	α lamellae	72	24	4
	η lamellae	5	90	5
Interparticle areas after ageing	matrix	1	1	99
	precipitates	22	64	14

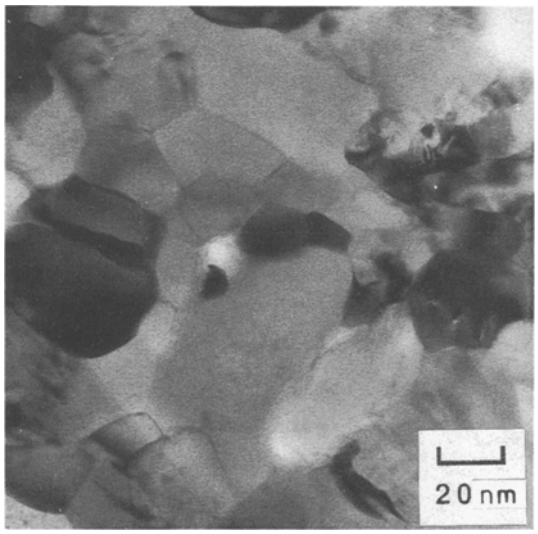

Figure 8 Appearance of the interparticle area in the as-stir-cast sample.

covering five grains. It is therefore considered that the phase constituting the interparticle area is mainly $CuZn_4$.

3.4. Effect of a high temperature ageing treatment

Fig. 9a shows a typical area of the primary α particles after ageing. Both elongated and spherical precipitates of similar dimensions to those in the as-cast sample (Fig. 6a) were observed. Some areas of the primary α particles, however, contained only spherical precipitates (Fig. 9b) indicating that in some areas the elongated precipitates had undergone complete spheroidization. When this was the case, much smaller precipitates (≈ 50 nm) could be seen in the background. It is likely that spheroidization of the long and thin precipitates was more nearly complete in the aged samples than in the as-cast samples although more observations of different areas would be needed to confirm this. Indeed, the diffraction conditions are identical for all the areas of the primary α seen in Fig. 9. The conditions are $g = (2\bar{2}0)$ near [1 1 1].

Composite diffraction patterns of the α matrix and of the precipitates were identical to those obtained for the as-cast sample (Fig. 6c) indicating that the precipitates were zinc. Thus, the microstructure of the α particles after ageing was very similar to that of the samples prior to ageing.

Fig. 10 is a portion of the interface between the α particle and the β eutectoid. As in the case of the as-stir-cast sample, some coarse zinc precipitates (≈ 1 μm) can be seen along the interface. A comparison of Fig. 10 with Fig. 6a from as-cast sample shows that the main change at the interface during ageing was the occurrence of copious precipitation in the α regions of the interface. Such precipitation also occurred in the α lamellae of the β eutectoid (marker B in Fig. 10). A higher magnification micrograph of one α lamella is shown in Fig. 11 along with a [1 1 1] diffraction pattern from the aluminium matrix. Clearly, the pattern is identical to those obtained for the primary α particles (Fig. 6) which shows that the precipitates formed in the α lamellae during ageing are zinc. X-ray microanalysis of α and η eutectoid lamellae showed that their chemical composition were identical for both the as-stir-cast and the aged samples (Table II). The only difference was that zinc precipitates formed in the α-fcc lamellae during ageing.

Ageing also led to a significant transformation of the interparticle areas. These areas, of a composition determined to be close to that of $CuZn_4$, in the as-cast condition transformed upon ageing into a matrix of zinc containing very little amounts of copper and aluminium in solution and a larger number of precipitates approximately 0.2 μm in size as shown in Fig. 12. In some cases, precipitates were actually sticking out from the edge of the hole of the foil thereby allowing X-ray analysis and electron diffraction of the precipitates without any contribution from the matrix. Both the chemical composition (Table II) and the indexation of the diffraction pattern show the precipitates to be the τ′ phase studied by Murphy [9] with a composition of 22Al–64Cu–14Zn and a rhombohedral structure with $a = b = c = 0.8676$ nm and $\alpha = \beta = \gamma = 27.41°$.

4. Discussions

The solidification conditions during stir casting are quite different from those during conventional casting. In stir casting, the percentage of primary particles,

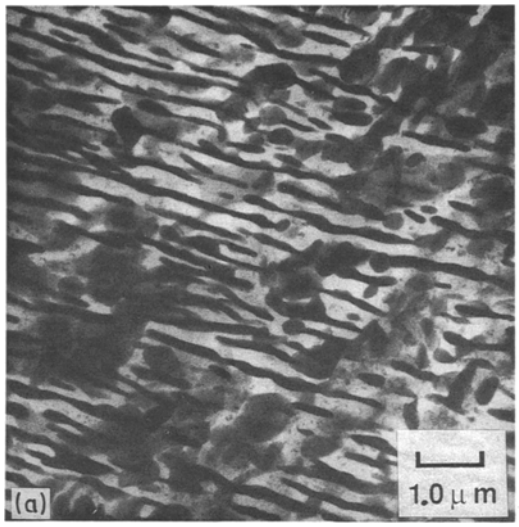

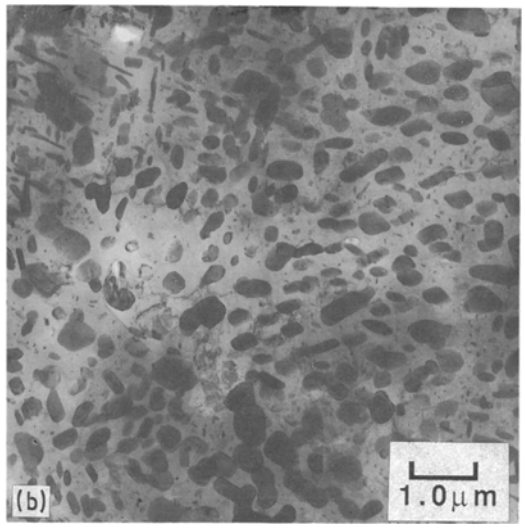

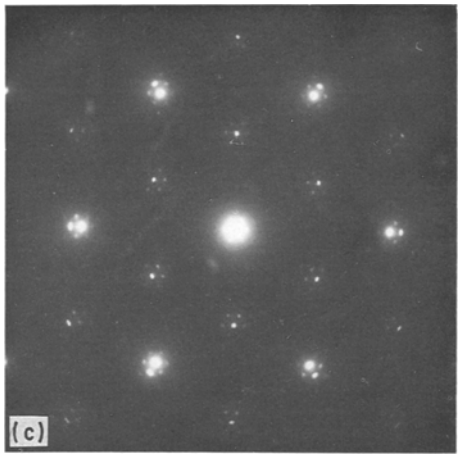

Figure 9 (a) Microstructure of the primary α particles after a high temperature ageing treatment. (b) Area of a primary α particle containing only spherical precipitates ($g = (2\bar{2}0)$ near [1 1 1]). Note the presence of very small precipitates (≈ 50 nm) in the background. (c) Diffraction pattern from the area shown in (b).

formed during the stirring stage, i.e. the α phase which is in the present study approximately 30% of the total volume of the alloy, is much larger than that obtained in dendritic cast material. In addition, the cooling rate of the stirring stage is generally low [15], i.e. between 1 to 10 °C min^{-1} with usually a holding time of a few minutes prior to casting. The influence of these casting parameters on the structure of stir-cast materials has been discussed in earlier work [4]. Thus under these conditions, the α phase supersaturation of the primary particles would not be as high as inside the dendrites of conventional casting. The subsequent heat treatment should not change its structure. On the other hand, the second stage of solidification of the slurry occurred when the liquid–solid metal was poured into the mould, i.e. at a temperature well below the liquidus. Therefore, the supersaturation of zinc content in the α lamellae must have been high. Subsequent heat treatment induced profound changes in the α lamellae by precipitation of the excess zinc. Mykura *et al.* [13] pointed out this decomposition reaction $\alpha_{supersaturated} \rightarrow \alpha + \eta$ as a short term transformation. As the presence of copper in solution increases the time of transformation [16], our results showed that it could hardly be achieved at room temperature so that heat treatments at a moderately raised temperature are needed to induce the reaction. As this transformation is associated with the slight contraction in the early stages of ageing, stir-cast materials with the presence of stable α primary particles are less influenced.

On the other hand, the long term phase transformation, which produce dimensional growth, are associated [13] with two distinct reactions. One is the four-phase reaction transforming the copper-rich metastable ε phase into the equilibrium τ′ phase as discussed in section 3.4. The other is due to the reduction of copper content in solution in the Zn-rich phase. In stir-cast alloy, copper is concentrated in the interparticle areas whereas the α primary particles and

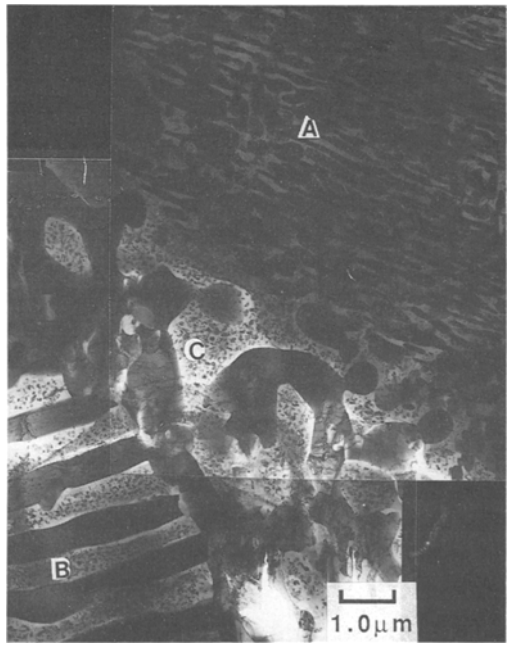

Figure 10 Micrograph of the interface between the primary particles and the β eutectoid after ageing. Copious precipitation occurred during ageing in the α regions of the interface (marker C) and in the α lamellae of the β eutectoid (marker B).

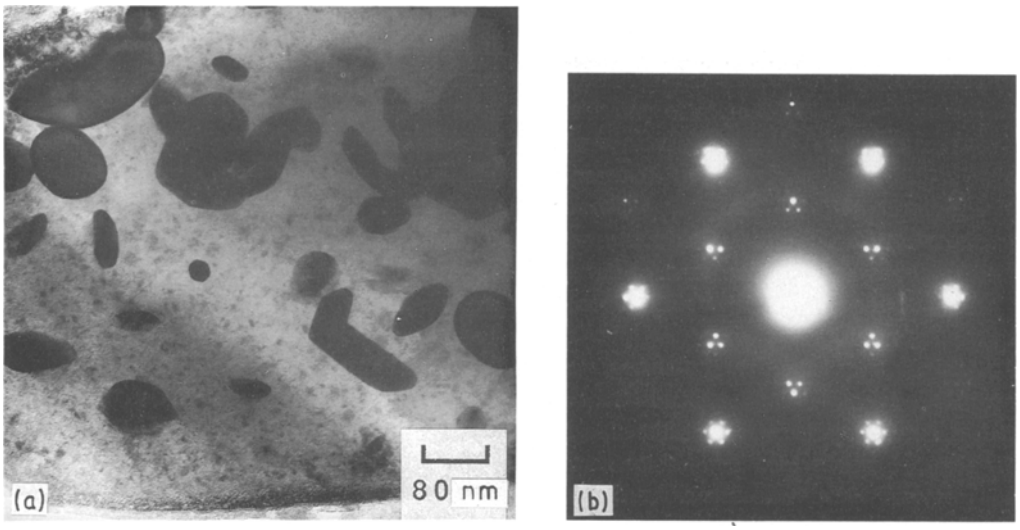

Figure 11 (a) TEM micrograph of an α lamella of the β eutectoid showing the extensive precipitation that occurred during ageing, (bright field image taken at the [1 1 1] zone axis). (b) [1 1 1] diffraction pattern from the aluminium matrix.

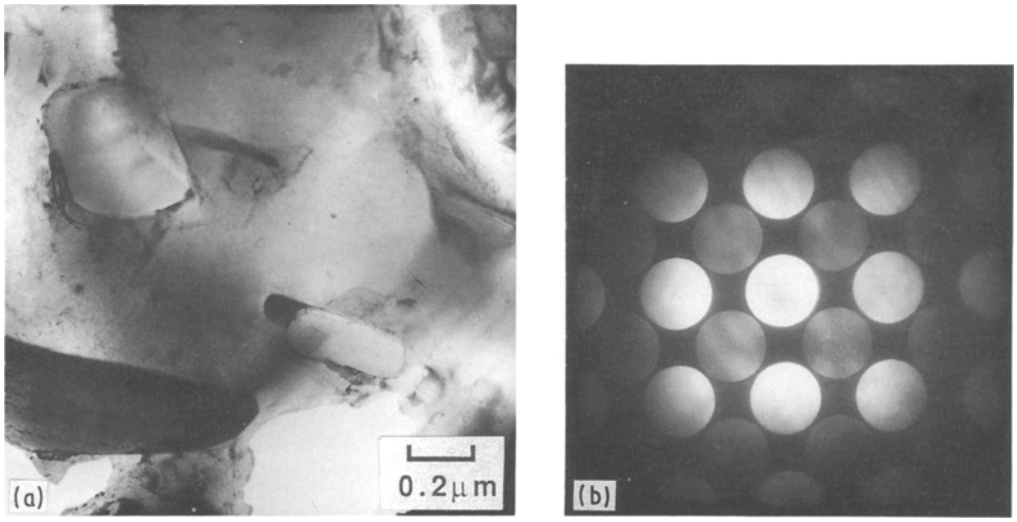

Figure 12 (a) Micrograph of the interparticle areas after ageing showing precipitates approximately 0.2 μm in size formed in a matrix of almost pure zinc. (b) Diffraction pattern from the precipitates shown in (a).

β constituent are leaner in copper than in the equivalent dendritic material and are by this fact less influenced by the η hcp growth. Therefore, the transformation of the interparticle areas with formation of τ′ as shown above seems to be the main reason for the growth in aged stir-cast materials.

5. Conclusions

Phase transformation of as-cast (dendritic and non-dendritic) ZA-27 alloy during isothermal treatment is the resultant process of decomposition of several supersaturated phases. In the first stage, the fcc aluminium-rich phase decomposes into the equilibrium η and α phases. Our results clearly show this decomposition reaction to be a short term transformation, inducing a slight contraction when the cast material is cooled down and/or in the early stages of ageing.

The long term phase transformations, which produce dimensional growth, are associated with the formation of equilibrium τ′ phase in the interdendritic (or interparticle) phases and to the reduction of copper content in solution in the Zn-rich phase.

In stir-casting material, the dimensional growth is slightly lower than that of conventionally cast material. It is tempting to associate this behaviour with the presence of more stable phases in primary particles and in the β constituent.

Acknowledgements

The authors would like to express their appreciation to Mr G. St-Amand for his technical assistance and their acknowledgements to Dr D. C. Briggs of CANMET for his invaluable advice.

References

1. "Engineering Properties of Zinc Alloys", 2nd edn (International Lead Zinc Res. Organization Inc., New York, 1981).
2. H. LeHUY, *J. Mater. Sci.* **23** (1988) 2843.
3. S. MURPHY, T. SAVASKAN and J. K. WHEELDON, in Proceedings Conference on Casting and Foundry Technology,

University of Aston, Birmingham, UK, (1981), Int. Congress on Metals Engineering, paper 7.
4. H. LeHUY, J. MASOUNAVE and J. BLAIN, *J. Mater. Sci.* **20** (1985) 105.
5. J. COLLOT, in Proceedings International Symposium on Zinc-Aluminium (ZA) Casting Alloys, 25th Annual Conference of Metal (1986), CIM Series 25–5/1, N° 1, 249–261, edited by G. P. Lewis, R. J. Barnhurst and C. A. Loong (Materials Engineering and Basic Sciences Sections of the Canadian Institute of Mining and Metallurgy).
6. R. GUERRIERO, J. B. PARSE and I. TANGERINI, *J. Mater. Sci.* **20** (1985) 229.
7. J. S. H. LO, S. DIONNE, L. DIGNARD-BAILEY, M. SAHOO and J. C. FARGE, in Proceedings Symposium on Processing of Ceramic and metal matrix Composites, Halifax, 1989, edited by H. Mostaghaci (Pergamon Press, 1989) p. 412.
8. J. LECOMTE-BECKERS, L. TERZIEV, J. WEGRIA and T. GREDAY, *J. Mater. Sci.* **20** (1985) 35.
9. S. MURPHY, *Metal Sci.* **9** (1975) 163.
10. D. B. WILLIAMS, "Practical Analytical Electron Microscopy in Materials Science" (Philips Electron Instrument Inc., Electron Optics Publ. Group, New-Jersey, 1984).
11. M. H. LORETTO, "Electron Beam Analysis of Materials" (Chapman and Hall, London, 1984).
12. J. E. WOOD, D. B. WILLIAMS and J. I. GOLDSTEIN, *J. Microscopy*, **133** (1984) 255.
13. N. MYKURA, Y. H. ZHU and S. MURPHY, *Canadian Met. Quart.* **25** (1986) 151.
14. "Phase Diagram", Metals Handbook, ASM, 8th edn, Vol. 8, (1973) pp. 390–391.
15. H. LeHUY, J. BLAIN and J. MASOUNAVE, *J. Mater. Sci.* **20** (1985) 143.
16. A. E. SMITH and G. A. HARE, *J. Inst. Metals* **101** (1973) 320.

Received 13 November
and accepted 1 December 1989